Nitrogen controlled iron catalyst phase during carbon nanotube growth

Bernhard C. Bayer, Carsten Baehtz, Piran R. Kidambi, Robert S. Weatherup, Clemens Mangler, Jani Kotakoski, Caroline J. L. Goddard, Sabina Caneva, Andrea Cabrero-Vilatela, Jannik C. Meyer, and Stephan Hofmann

Citation: Applied Physics Letters **105**, 143111 (2014); doi: 10.1063/1.4897950
View online: http://dx.doi.org/10.1063/1.4897950
View Table of Contents: http://scitation.aip.org/content/aip/journal/apl/105/14?ver=pdfcov
Published by the AIP Publishing

Nitrogen controlled iron catalyst phase during carbon nanotube growth

Bernhard C. Bayer,[1,2,a)] Carsten Baehtz,[3] Piran R. Kidambi,[1] Robert S. Weatherup,[1] Clemens Mangler,[2] Jani Kotakoski,[2] Caroline J. L. Goddard,[4] Sabina Caneva,[1] Andrea Cabrero-Vilatela,[1] Jannik C. Meyer,[2] and Stephan Hofmann[1]
[1]*Department of Engineering, University of Cambridge, Cambridge CB3 0FA, United Kingdom*
[2]*Faculty of Physics, University of Vienna, A-1090 Vienna, Austria*
[3]*Institute of Ion Beam Physics and Materials Research, Helmholtz-Zentrum Dresden-Rossendorf, D-01314 Dresden, Germany*
[4]*Department of Materials Science and Metallurgy, University of Cambridge, Cambridge CB3 0FS, United Kingdom*

(Received 26 August 2014; accepted 27 September 2014; published online 9 October 2014)

Close control over the active catalyst phase and hence carbon nanotube structure remains challenging in catalytic chemical vapor deposition since multiple competing active catalyst phases typically co-exist under realistic synthesis conditions. Here, using *in-situ* X-ray diffractometry, we show that the phase of supported iron catalyst particles can be reliably controlled via the addition of NH_3 during nanotube synthesis. Unlike polydisperse catalyst phase mixtures during H_2 diluted nanotube growth, nitrogen addition controllably leads to phase-pure γ-Fe during pre-treatment and to phase-pure Fe_3C during growth. We rationalize these findings in the context of ternary Fe-C-N phase diagram calculations and, thus, highlight the use of pre-treatment- and add-gases as a key parameter towards controlled carbon nanotube growth. © *2014 AIP Publishing LLC*.
[http://dx.doi.org/10.1063/1.4897950]

In order to unlock the full application potential of the exceptional electronic, thermal, and mechanical properties of carbon nanotubes (CNTs), a scalable synthesis technique is required that also allows close control over the structure of the growing nanotubes. Catalytic chemical vapor deposition (CVD) in which metallic nanoparticles act as templating seeds for CNT growth has reached maturity in terms of industrial scalability and process integration but still has major shortcomings in terms of structural selectivity during growth. For instance, to date selective growth of CNTs with specific narrow sets of chiralities remains limited.[1–3] As the structure of the nanotube is largely defined at the point of nucleation[2,4] and thereby templated by the state of the catalyst at this point, the first requirement for control over nanotube structures is stringent control over the phase and structure of the catalyst. Such control however remains equally limited, as multiple competing active catalyst phases co-exist under typical CVD conditions.[5,6] Kinetic effects thereby dominate the evolution of non-equilibrium catalyst phase mixtures during the CNT CVD process. For archetypal, widely used Fe catalysts,[7–9] it has been shown that minor carbonaceous background contamination levels typically present in CVD reactors can lead to mixtures of α-Fe and γ-Fe nanoparticles during pre-treatment and that upon subsequent hydrocarbon exposure at 750 °C, these phase mixtures further evolve into complex metallic Fe and iron-carbide mixtures.[5] In general, to controllably enforce a single active catalyst phase remains as a key challenge towards structurally controlled carbon nanotube growth.

Here, we show that the phase of alumina supported Fe catalyst particles can be reliably controlled via the addition of nitrogen (in the form of NH_3) during the CNT CVD process. Unlike catalyst phase mixtures during H_2 diluted CNT CVD,[5] *in-situ* X-ray diffractometry (XRD) shows that nitrogen addition controllably leads to phase-pure γ-Fe catalysts during pre-treatment and to phase-pure Fe-carbide (Fe_3C) during growth. We rationalize these findings in terms of accessible pathways across ternary Fe-C-N phase diagram calculations and discuss implications for controlling CNT structure and chirality.

We use a synchrotron-based *in-situ* XRD setup[5,9–13] in a grazing incidence geometry and adopt CNT CVD conditions that are widespread in literature.[7–9] We employ evaporated Fe 8 nm catalyst films (which restructure into nanoparticles upon pre-treatment) on Al_2O_3 coated[9,10] Si wafer support. The use of the comparably thick Fe 8 nm films is necessary to obtain acceptable XRD counting rates in our *in-situ* XRD experiments. Unlike prior typically used H_2 based dilution, NH_3 (ammonia) is used as the pre-treatment- and add-gas. Samples are pre-treated in a NH_3:Ar atmosphere at 750 °C and C_2H_2 is subsequently added to the NH_3:Ar mixture for CNT growth. See supplementary material for further details on methods.[14]

Figure 1 shows the phase evolution for these Fe 8 nm catalysts throughout salient stages of the CVD process. The phase of the as deposited (stage I) Fe samples is identified as α-Fe (body-centered-cubic Fe, ferrite). During pre-treatment (stage II), when we heat to 750 °C in NH_3:Ar, we find a complete phase transition from α-Fe to phase-pure γ-Fe (face-centered-cubic, austenite).

Upon C_2H_2 addition (stage III), we observe the growth of CNTs (evidenced by the appearance of the graphite reflection at ~18° in Figure 1 and corroborated by further *ex-situ* characterization in Figure 2). Concurrently, the catalyst phase changes from γ-Fe to Fe_3C iron carbide (orthorhombic

a)Author to whom correspondence should be addressed. Electronic mail: bernhard.bayer@univie.ac.at

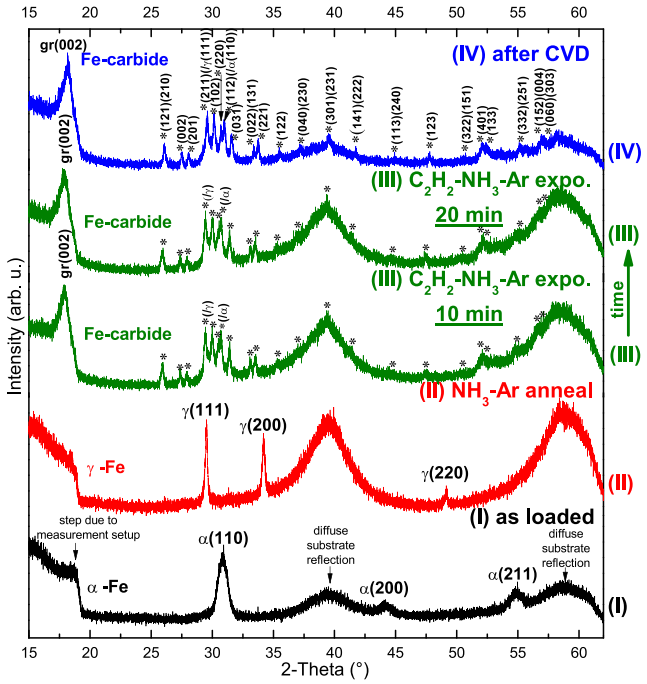

FIG. 1. *In-situ* diffractograms for each CVD process step (I-IV). "gr" designates reflections from graphitic material, "α" from α-Fe, "γ" from γ-Fe, and "*" from Fe_3C (Miller indices indicated). We find that during NH_3:Ar pretreatment, the as deposited α-Fe is fully transformed into γ-Fe and that during subsequent C_2H_2 feeding CNTs grow from Fe_3C. The majority catalyst phase is indicated for each processing step next to the respective scans. The X-ray wavelength was 1.078 Å. The broad background step at ~19° is related to the entrance/exit geometry of X-ray windows in the reaction cell. The broad background humps around 40° and 58°, which increase in intensity with increasing temperature, are due to diffuse scattering from the amorphous support. We note that the measured reflection positions shift slightly between room temperature and 750 °C due to thermal expansion, which was not corrected for in the plot.

cementite θ-Fe_3C). Qualitative phase analysis indicates phase-pure Fe_3C during growth (based on the absence of any secondary reflections for either γ-Fe or α-Fe). Using quantitative Rietveld refinement, we set an upper limit to the maximum contributions of γ-Fe and α-Fe that could be "hidden" in the signal noise: We can force only a maximum of up to 8 wt. % and 12 wt. % of γ-Fe and α-Fe, respectively, into the refinements, i.e., a minimum of >80 wt. % Fe_3C is confirmed. When measuring repeated XRD scans during C_2H_2 exposure, the Fe_3C pattern remains unchanged as the dominant signal, implying that the Fe_3C remains structurally stable (i.e., does not undergo phase changes with time), while concurrently catalyzing CNT growth.

We find that the Fe_3C phase is also preserved during cooling in vacuum after C_2H_2 exposure (stage IV). This allows us to compare our XRD phase assignment with point-localized *ex-situ* transmission electron microscopy (TEM) and selected area electron diffraction (SAED) analysis (Figure 2(a)): Identifying the phase of 13 catalyst particles, which are attached to the ends of CNTs (inset in Figure 2(a)) by TEM/SAED, we match 12 of the particles exclusively to Fe_3C (with one remaining particle matching to either Fe_3C or α-Fe). Thus, the *ex-situ* TEM/SAED analysis is in excellent agreement with our *in-situ* XRD-based identification of Fe_3C as the catalyst state. We further corroborate our phase analysis using aberration-corrected scanning transmission electron microscopy (STEM), which allows phase identification based on direct lattice-resolved imaging of the catalyst particles. For instance, in Figure 2(b), we identify a lattice

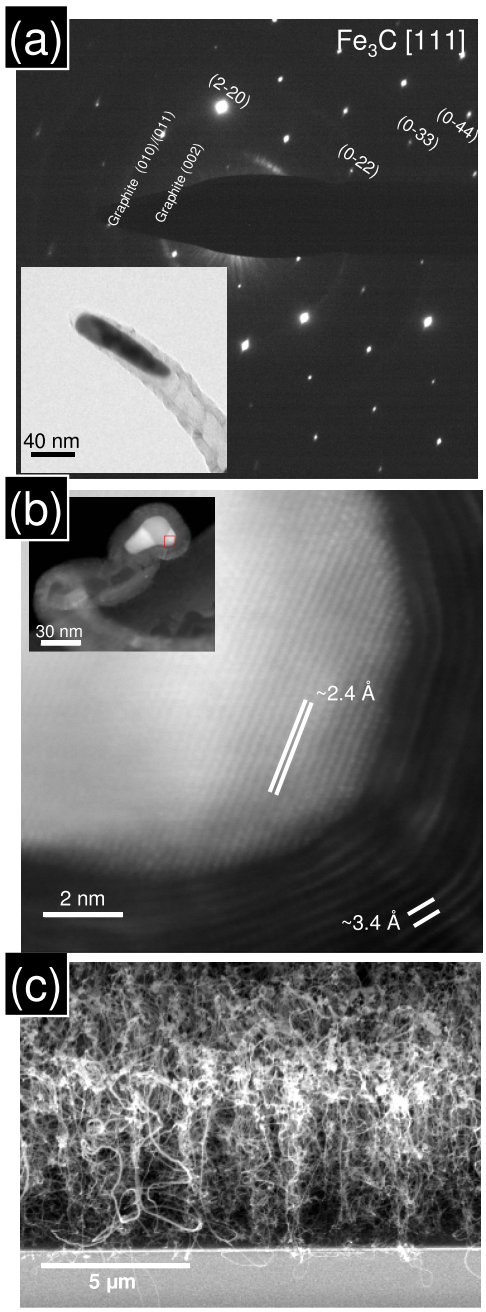

FIG. 2. (a) SAED pattern of the catalyst particle that is shown in the TEM bright field image in the inset. The spot pattern is indexed to orthorhombic Fe_3C viewed along the [111] zone axis. We note that for the (2–20) reciprocal vector direction double diffraction effects are observed. The diffraction rings are assigned to the graphitic signal from the carbon nanotube walls. (b) Lattice-resolved STEM image of a catalyst particle edge and adjacent nanotube graphene layers. The measured lattice distance of ~2.4 Å excludes α-Fe and γ-Fe (as metallic phases have maximum lattice spacings of <2.15 Å) and is consistent with several hkl planes in Fe_3C (e.g. (200), (121), or (210)). The spacing of the graphene layers in the CNT walls is, as expected, ~3.4 Å. The corresponding lower magnification overview STEM image in the inset shows that this particular catalyst particle is polycrystalline in nature, exhibiting three grains (visible via slight differences in image contrast). Lattice-resolved analysis of the three grains shows all of them exhibiting lattice fringes consistent with Fe_3C (where two grains are unambiguously and exclusively matched to Fe_3C). (c) Scanning electron microscopy (SEM) image of the grown CNTs from the catalyst evolution in Figure 1, showing vertical alignment of tubes ("CNT forest").

spacing in the catalyst particle of ~2.4 Å, which excludes both α-Fe and γ-Fe, as both metallic phases have maximum lattice spacings of <2.15 Å. In turn, ~2.4 Å is fully consistent with Fe_3C. Interestingly, the catalyst particle for the particular nanotube in Figure 2(b) was found to be polycrystalline, as the lower magnification STEM image in the inset of Figure 2(b) shows contrast variations within the catalyst particle, indicative of three separate, differently oriented grains (with lattice fringes all consistent with Fe_3C). In general, we observe a mixture of single-crystalline and polycrystalline catalyst particles in our measurements, where STEM analysis of 8 individual catalyst particles identified the lattice fringes for all measured particles as being consistent with Fe_3C (with a majority being unambiguously identified as Fe_3C due to lattice fringe distances of >2.15 Å). Combined, the post-CVD *ex-situ* TEM/SAED/STEM data fully corroborate our *in-situ* XRD assignment of Fe_3C as the active catalyst phase during our CNT growth with NH_3.

On the Al_2O_3-covered wafer support the nanotubes exhibit vertical alignment ("forest" morphology, Figure 2(c)) similar to standard CNT growth in the literature under comparable CVD conditions,[7–9] albeit at a lower areal number density of tubes and a somewhat lower degree of vertical alignment. Microscopically, the tubes are of multi-walled structure, with a mixture of straight tube sections (Figure S1a) and of tubes exhibiting compartments and bamboo-type growth morphologies (Figure S1b).[14] The outer CNT diameter distribution has a median value of 24 nm (mean: 28 nm, standard deviation: 15 nm, minimum: 9 nm, maximum: 81 nm, measured over 100 tubes). These rather broad diameter and morphology ranges and the comparably low degree of vertical alignment are a result of the comparably thick catalyst films (Fe 8 nm), which are necessary to obtain acceptable XRD counting rates and which thereby result in a trade-off from monodisperse tube properties.

In previous work,[5] we used H_2 as pre-treatment- and add-gas for similar samples and CVD conditions, which allows here for a detailed comparative discussion of the effects of NH_3 addition. H_2 dilution led to complex catalyst phase mixtures during CVD pre-treatment and growth (Figure 3(a)) in contrast to the now obtained single-phased catalysts. Pre-treatment with H_2:Ar at 750 °C (stage II) resulted in mixtures of α-Fe and γ-Fe. The unexpected formation of γ-Fe with H_2 at 750 °C (transition temperature α-Fe to γ-Fe for pure Fe is 912 °C[15]) was ascribed to adventitious carbon contamination (from sample transport in ambient air and residual carbon in the CVD system), which resulted in carbon uptake in the catalyst upon annealing, thereby lowering the transition temperature for γ-Fe formation down to 727 °C via an eutectoid phase boundary in the Fe-C phase diagram.[15] In the subsequent growth step with H_2:C_2H_2:Ar (stage III), the α-Fe/γ-Fe mixtures further evolved into three-phase mixtures of α-Fe, γ-Fe, and Fe_3C iron carbide, where both the metallic iron and the iron carbide were active catalysts. We argued that these polydisperse catalyst phase mixtures when using H_2 result from the complex interplay of the α-Fe/γ-Fe phase ratios from pre-treatment and the multiple kinetically accessible pathways for large nanoparticle ensembles when growth conditions are close to the eutectoid triple-phase boundaries of α-Fe, γ-Fe, and Fe_3C/graphite (eutectoids at 727 °C/3.46 at. % carbon and 740 °C/2.97 at. % carbon for Fe-Fe_3C and Fe-graphite, respectively[15]). Similar to the many disparate previous results in the wider literature,[16–49] our previous work with H_2 highlighted the complexity of Fe-catalyzed CNT growth.[5]

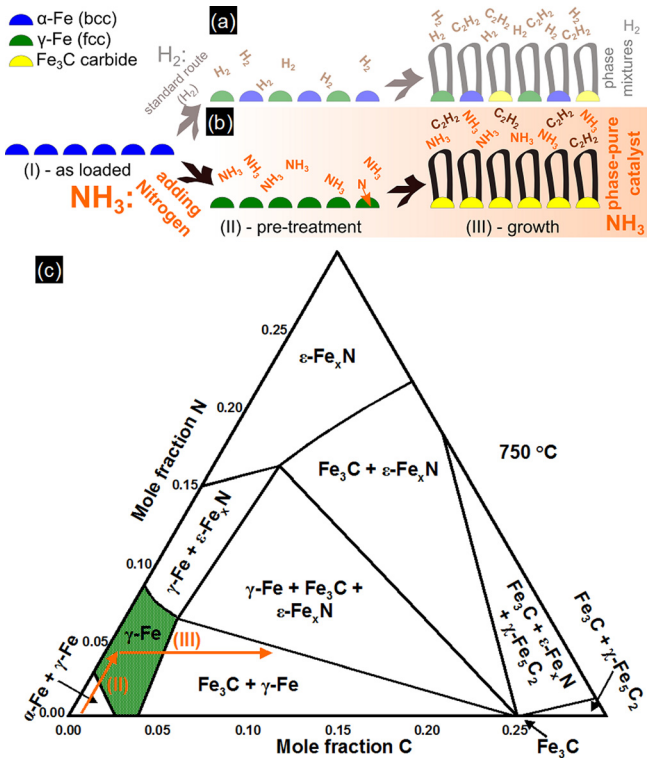

FIG. 3. (a) and (b) Schematic sketches of the observed catalyst phase evolution at 750 °C: (a) "standard" reference conditions with H_2 as pre-treatment- and add-gas during CNT growth (as in Ref. 5), resulting in uncontrolled phase mixtures of α-Fe/γ-Fe (during pre-treatment) and of α-Fe/γ-Fe/Fe_3C (during growth). In contrast, in (b) introducing NH_3 as the pre-treatment- and add-gas controllably selects phase-pure γ-Fe and phase-pure Fe_3C as the active catalyst phases during pre-treatment and growth, respectively. (c) Calculated ternary phase diagram of the Fe-C-N system at 750 °C. Possible exemplary compositional trajectories during pre-treatment (II) and growth (III) are indicated by orange arrows. The single-phase γ-Fe phase field is highlighted in green.

Now by adding nitrogen in the form of NH_3 into the growth atmosphere, we achieve close control over the catalyst phase (Figure 3(b)). Pre-treatment of the as deposited α-Fe catalyst in NH_3 at 750 °C results in phase-pure γ-Fe particles (instead of mixtures of α-Fe/γ-Fe as with H_2). As NH_3 is known to dissociate on Fe under the given temperature/pressure conditions,[50] we suggest that dissociated nitrogen on the catalyst surface diffuses into the Fe nanoparticles (Figure 3(b)). This assertion is corroborated by formation of Fe-nitrides (ε-Fe_xN) when applying higher NH_3 partial pressures (×10, Figure S2).[14] Our thermodynamic calculations of the ternary Fe-C-N system at 750 °C (Figure 3(c)) help to rationalize the effect of nitrogen uptake on the Fe phase evolution: For pristine Fe and low carbon content Fe (possible from, e.g., adventitious carbon contamination[5]), we find that addition of N during pre-treatment (orange trajectory (II) in Figure 3(c)) leads to phase-pure γ-Fe formation, as experimentally observed. This is also consistent with published binary Fe-N phase diagram data,[51] where the uptake of N into the Fe bulk strongly reduces the α-Fe → γ-Fe transition

temperature (from 912 °C in pure Fe[15] down to an eutectoid minimum of 592 °C at 8.8 at. % N.[51]) Thus, by co-feeding nitrogen during pre-treatment we have prevented the formation of the previously[5] obtained α-Fe/γ-Fe mixtures during pre-treatment by thermodynamically forcing the system into a defined phase-pure γ-Fe state (green area in Figure 3(c)) at otherwise constant CVD conditions and irrespective of initial minor residual carbon contamination.[5]

Equally, during exposure to the hydrocarbon source in the growth stage (orange trajectory (III) in Figure 3(c)), we observed phase-pure Fe_3C catalyst particles when using NH_3 (in contrast to the γ-Fe/α-Fe/Fe_3C mixtures when using H_2[5]). Thus, co-feeding of nitrogen also drastically changed the phase evolution of the catalyst during the growth stage, indicating that nitrogen addition stabilizes Fe_3C. This observation is in good agreement with previously published phase stabilities in the ternary Fe-C-N system as a function of nitrogen and carbon activities ("Lehrer diagrams")[52,53] and also with recent first principle calculations on the stabilizing effect of N addition on Fe_3C.[54] Our own thermodynamic calculations in Figure 3(c) also show that the phase fraction of Fe_3C is incrementally increasing by N addition for a range of C contents. We note however that while the Fe_3C fraction in the γ-Fe/Fe_3C two phase field incrementally increases with N content, we do not calculate a phase-pure Fe_3C region in the considered (C,N) compositional range (unlike for γ-Fe). This implies that kinetic effects, nucleation barriers, etc., also have a remaining impact on the observed phase-purity of Fe_3C in our *in-situ* data.

Our findings align with the wider metallurgy literature,[55] where treatment of Fe with carbonaceous gases in NH_3-containing environments ("nitro-carburizing") is known to induce massive growth of phase-pure Fe_3C layers compared to formation of only metallic iron and graphite layers in NH_3-free carburizing environments.[56] The observed stability of Fe_3C during nanotube growth in the presence of nitrogen is also in line with previous point-localized TEM observations by Koziol *et al.*,[27,57–59] where our integral *in-situ* XRD data further extends the beneficial effects of nitrogen addition towards structural control of large nanoparticle ensembles not only during growth but also during pre-treatment, i.e., towards a controlled γ-Fe catalyst state at the point of initial hydrocarbon exposure just before CNT nucleation.

For higher NH_3 partial pressures ($\times 10$), we observed the additional formation of Fe-nitrides (ε-Fe_xN) during pre-treatment (Figure S2),[14] resulting in a non-phase-pure mixture of γ-Fe and ε-Fe_xN prior C_2H_2 exposure. ε-Fe_xN formation for higher N content is again in good agreement with our thermodynamic calculations (Figure 3(c)) and also published phase diagram data.[51] The additional formation of ε-Fe_xN at higher NH_3 pressures implies that in order to grow CNTs from a phase-pure catalyst regime, a certain window of nitrogen and carbon activities (i.e., NH_3 and C_2H_2 partial pressures) has to be maintained. This is analogous to the requirements in nitro-carburizing of metallurgical steels, where also a balance of the gaseous nitrogen and carbon sources has to be kept to grow phase-pure Fe_3C layers instead of carbide/nitride/metal/graphite mixtures.[53,55,56] Equally, too low NH_3 pressures may also result in a non-phase-pure Fe catalyst state (Figure 3(c)).[5]

Depending on CVD conditions (e.g., temperatures, pressures, feedstocks, etc.), various Fe phases have been shown in the literature to be active for CNT growth including the liquid[16–19,45] and solid metallic[20,21,38] state, as well as solid structural carbides[22–24,34–37,46] and solid particles undergoing transient bulk carbide formation/disintegration ("metal dusting mechanism").[35,39–41,60,61] Often complex non-phase-pure mixtures of these active catalyst states are reported.[5,17,28,30–33] The structural stability of Fe_3C observed here in repeated *in-situ* XRD scans during growth (Figure 1, stage III) largely excludes for our conditions, a transient bulk Fe_3C formation/disintegration process (in which the entire Fe_3C particles would only act as an intermediate species and, thus, disintegrate to metallic iron upon CNT nucleation[35,39–41]). Instead, our *in-situ* XRD data here demonstrate a vapor-solid-solid (VSS) CNT growth mechanism from phase-pure stable solid Fe_3C catalysts under our NH_3-containing CVD conditions at 750 °C.

While the multi-walled, partly defective nature of the as-grown CNTs in our *in-situ* XRD studies (which is a direct result of the comparably thick catalysts films necessary to obtain acceptable XRD counting rates) does not allow us to comment on statistically relevant differences in obtained tube morphologies from the presence of nitrogen, we note that our *in-situ* observations are in good agreement with other recent work on the impact of gaseous pre-treatment- and add-elements in chiral-selective single-walled carbon nanotube (SWNT) growth.[2,4,62–66] In this context, e.g., we have recently shown that the addition of NH_3 to the pre-treatment atmosphere for SWNT CVD narrows and downshifts diameter and chiral distributions in cobalt-catalyzed SWNT growth.[4] In line with our current observations, we argued that this was related to nitrogen-induced changes in the cobalt catalyst structure/faceting, which translate to a change in nucleating SWNT chiralities.[4]

In summary, using *in-situ* X-ray diffractometry, we have directly demonstrated how the addition of a pre-treatment- and add-gas changes the evolution of Fe-catalysts in typical and industrially scalable CNT CVD conditions. Instead of polydisperse catalyst phase mixtures in commonly employed H_2 diluted CVD, the addition of nitrogen (in the form of NH_3) controllably leads to phase-pure γ-Fe catalysts during pre-treatment and to phase-pure Fe-carbide (Fe_3C) during growth. Our findings highlight that pre-treatment- and add-gases are a key optimization parameter towards structurally controlled CNT growth via structural control of the active catalyst phase.

B.C.B. acknowledges a Research Fellowship at Hughes Hall, Cambridge. B.C.B. and J.C.M. acknowledge support from the Austrian Science Fund (FWF): P25721-N20. P.R.K. acknowledges funding from the Cambridge Commonwealth Trust. R.S.W. acknowledges a Research Fellowship from St. John's College, Cambridge. J.K. acknowledges funding from the Austrian Science Fund (FWF): M1481-N20. A.C.V. acknowledges the Conacyt Cambridge Scholarship and Roberto Rocca Fellowship. S.H. acknowledges funding from ERC Grant InsituNANO (No. 279342). We acknowledge the European Synchrotron Radiation Facility (ESRF) for provision of synchrotron

radiation and we thank the staff for assistance in using beamline BM20/ROBL. We want to thank Daniel Huber (Böhler Schmiedetechnik GmbH & Co KG, Austria) for fruitful discussions.

[1]F. Yang, X. Wang, D. Zhang, J. Yang, D. Luo, Z. Xu, J. Wei, J.-Q. Wang, Z. Xu, and F. Peng, Nature **510**, 522 (2014).
[2]A. R. Harutyunyan, G. Chen, T. M. Paronyan, E. M. Pigos, O. A. Kuznetsov, K. Hewaparakrama, S. M. Kim, D. Zakharov, E. A. Stach, and G. U. Sumanasekera, Science **326**, 116 (2009).
[3]M. Fouquet, B. C. Bayer, S. Esconjauregui, R. Blume, J. H. Warner, S. Hofmann, R. Schlögl, C. Thomsen, and J. Robertson, Phys. Rev. B **85**, 235411 (2012).
[4]M. Fouquet, B. C. Bayer, S. Esconjauregui, C. Thomsen, S. Hofmann, and J. Robertson, J. Phys. Chem. C **118**, 5773 (2014).
[5]C. T. Wirth, B. C. Bayer, A. D. Gamalski, S. Esconjauregui, R. S. Weatherup, C. Ducati, C. Baehtz, J. Robertson, and S. Hofmann, Chem. Mater. **24**, 4633 (2012).
[6]Y. Kohigashi, H. Yoshida, Y. Homma, and S. Takeda, Appl. Phys. Lett. **105**, 073108 (2014).
[7]A. J. Hart and A. H. Slocum, J. Phys. Chem. B **110**, 8250 (2006).
[8]K. Hata, D. N. Futaba, K. Mizuno, T. Namai, M. Yumura, and S. Iijima, Science **306**, 1362 (2004).
[9]B. C. Bayer, S. Hofmann, C. Castellarin-Cudia, R. Blume, C. Baehtz, S. Esconjauregui, C. T. Wirth, R. A. Oliver, C. Ducati, A. Knop-Gericke, R. Schlögl, A. Goldoni, C. Cepek, and J. Robertson, J. Phys. Chem. C **115**, 4359 (2011).
[10]B. C. Bayer, S. Sanjabi, C. Baehtz, C. T. Wirth, S. Esconjauregui, R. S. Weatherup, Z. H. Barber, S. Hofmann, and J. Robertson, Thin Solid Films **519**, 6126 (2011).
[11]B. C. Bayer, C. Zhang, R. Blume, F. Yan, M. Fouquet, C. T. Wirth, R. S. Weatherup, L. Lin, C. Baehtz, R. A. Oliver, A. Knop-Gericke, R. Schlögl, S. Hofmann, and J. Robertson, J. Appl. Phys. **109**, 114314 (2011).
[12]P. R. Kidambi, B. C. Bayer, R. Blume, Z.-J. Wang, C. Baehtz, R. S. Weatherup, M.-G. Willinger, R. Schloegl, and S. Hofmann, Nano Lett. **13**, 4769 (2013).
[13]R. S. Weatherup, C. Baehtz, B. Dlubak, B. C. Bayer, P. R. Kidambi, R. Blume, R. Schloegl, and S. Hofmann, Nano Lett. **13**, 4624 (2013).
[14]See supplementary material at http://dx.doi.org/10.1063/1.4897950 for detailed description of methods, scanning transmission electron microscopy images of typical CNT morphologies and *in-situ* diffractogram during pre-treatment in 10× higher NH_3 partial pressure.
[15]H. Okamoto, J. Phase Equilibria **13**, 543 (1992).
[16]R. Baker, P. Harris, R. Thomas, and R. Waite, J. Catal. **30**, 86 (1973).
[17]V. Heresanu, C. Castro, J. Cambedouzou, M. Pinault, O. Stephan, C. Reynaud, M. Mayne-L'Hermite, and P. Launois, J. Phys. Chem. C **112**, 7371 (2008).
[18]A. R. Harutyunyan, E. Mora, T. Tokune, K. Bolton, A. Rosén, A. Jiang, N. Awasthi, and S. Curtarolo, Appl. Phys. Lett. **90**, 163120 (2007).
[19]T. Ichihashi, J. Fujita, M. Ishida, and Y. Ochiai, Phys. Rev. Lett. **92**, 215702 (2004).
[20]J. A. Rodríguez-Manzo, M. Terrones, H. Terrones, H. W. Kroto, L. Sun, and F. Banhart, Nat. Nanotechnol. **2**, 307 (2007).
[21]S. Hofmann, R. Sharma, C. Ducati, G. Du, C. Mattevi, C. Cepek, M. Cantoro, S. Pisana, A. Parvez, F. Cervantes-Sodi, A. C. Ferrari, R. Dunin-Borkowski, S. Lizzit, L. Petaccia, A. Goldoni, and J. Robertson, Nano Lett. **7**, 602 (2007).
[22]H. Yoshida, S. Takeda, T. Uchiyama, H. Kohno, and Y. Homma, Nano Lett. **8**, 2082 (2008).
[23]R. Sharma, E. Moore, P. Rez, and M. M. Treacy, Nano Lett. **9**, 689 (2009).
[24]S. Mazzucco, Y. Wang, M. Tanase, M. Picher, K. Li, Z. Wu, S. Irle, and R. Sharma, J. Catal. **319**, 54 (2014).
[25]X.-Y. Liu, B.-C. Huang, and N. J. Coville, Carbon **40**, 2791 (2002).
[26]Y. J. Jung, B. Wei, R. Vajtai, P. M. Ajayan, Y. Homma, K. Prabhakaran, and T. Ogino, Nano Lett. **3**, 561 (2003).
[27]C. Ducati, K. Koziol, S. Friedrichs, T. J. Yates, M. S. Shaffer, P. A. Midgley, and A. H. Windle, Small **2**, 774 (2006).
[28]Z. He, J.-L. Maurice, A. Gohier, C. S. Lee, D. Pribat, and C. S. Cojocaru, Chem. Mater. **23**, 5379 (2011).
[29]A. K. Schaper, H. Hou, A. Greiner, and F. Phillipp, J. Catal. **222**, 250 (2004).
[30]R. Philippe, B. Caussat, A. Falqui, Y. Kihn, P. Kalck, S. Bordère, D. Plee, P. Gaillard, D. Bernard, and P. Serp, J. Catal. **263**, 345 (2009).
[31]Y. Homma, Y. Kobayashi, T. Ogino, D. Takagi, R. Ito, Y. J. Jung, and P. M. Ajayan, J. Phys. Chem. B **107**, 12161 (2003).
[32]S. M. Kim, C. L. Pint, P. B. Amama, D. N. Zakharov, R. H. Hauge, B. Maruyama, and E. A. Stach, J. Phys. Chem. Lett. **1**, 918 (2010).
[33]V. Pichot, P. Launois, M. Pinault, M. Mayne-L'Hermite, and C. Reynaud, Appl. Phys. Lett. **85**, 473 (2004).
[34]K. Nishimura, N. Okazaki, L. Pan, and Y. Nakayama, Jpn. J. Appl. Phys. **43**, L471 (2004).
[35]C. Emmenegger, J.-M. Bonard, P. Mauron, P. Sudan, A. Lepora, B. Grobety, A. Züttel, and L. Schlapbach, Carbon **41**, 539 (2003).
[36]P. Landois, S. Rouziére, M. Pinault, D. Porterat, C. Mocuta, E. Elkaim, M. Mayne–L'Hermite, and P. Launois, Phys. Status Solidi B **248**, 2449 (2011).
[37]V. L. Kuznetsov, D. V. Krasnikov, A. N. Schmakov, and K. V. Elumeeva, Phys. Status Solidi B **249**, 2390 (2012).
[38]S. Hofmann, R. Blume, C. T. Wirth, M. Cantoro, R. Sharma, C. Ducati, M. Haüvecker, S. Zafeiratos, P. Schnoerch, A. Oestereich, D. Teschner, M. Albrecht, A. Knop-Gericke, R. Schlögl, and J. Robertson, J. Phys. Chem. C **113**, 1648 (2009).
[39]H. Kim and W. Sigmund, Carbon **43**, 1743 (2005).
[40]P. De Bokx, A. Kock, E. Boellaard, W. Klop, and J. W. Geus, J. Catal. **96**, 454 (1985).
[41]Z. Zeng and K. Natesan, Chem. Mater. **17**, 3794 (2005).
[42]D.-M. Tang, C. Liu, W.-J. Yu, L.-L. Zhang, P.-X. Hou, J.-C. Li, F. Li, Y. Bando, D. Golberg, and H.-M. Cheng, ACS Nano **8**, 292 (2014).
[43]R. Baker, J. Alonzo, J. Dumesic, and D. Yates, J. Catal. **77**, 74 (1982).
[44]A. S. Anisimov, A. G. Nasibulin, H. Jiang, P. Launois, J. Cambedouzou, S. D. Shandakov, and E. I. Kauppinen, Carbon **48**, 380 (2010).
[45]R. Rao, N. Pierce, D. Liptak, D. Hooper, G. Sargent, S. Semaitin, S. Curtarolo, A. R. Harutyunyan, and B. Maruyama, ACS Nano **7**, 1100 (2013).
[46]A. Sacco, Jr., P. Thacker, T. N. Chang, and A. T. Chiang, J. Catal. **85**, 224 (1984).
[47]J.-Y. Raty, F. Gygi, and G. Galli, Phys. Rev. Lett. **95**, 096103 (2005).
[48]A. J. Page, H. Yamane, Y. Ohta, S. Irle, and K. Morokuma, J. Am. Chem. Soc. **132**, 15699 (2010).
[49]A. J. Page, S. Minami, Y. Ohta, S. Irle, and K. Morokuma, Carbon **48**, 3014 (2010).
[50]M. Grunze, F. Bozso, G. Ertl, and M. Weiss, Appl. Surf. Sci. **1**, 241 (1978).
[51]H. Wriedt, N. Gokcen, and R. Nafziger, Bull. Alloy Phase Diagr. **8**, 355 (1987).
[52]H. Du, J. Phase Equilibria **14**, 682 (1993).
[53]E. J. Mittemeijer, in *ASM Handbook Steel Heat Treating Fundamentals and Processes*, edited by J. Dossett and G. E. Totten (ASM International, 2013).
[54]O. Y. Gutina, N. Medvedeva, I. Shein, A. Ivanovskii, and J. Medvedeva, Phys. Status Solidi B **246**, 2167 (2009).
[55]D. Jack and K. Jack, Mater. Sci. Eng. **11**, 1 (1973).
[56]T. Gressmann, M. Nikolussi, A. Leineweber, and E. Mittemeijer, Scr. Mater. **55**, 723 (2006).
[57]S. W. Pattinson, V. Ranganathan, H. K. Murakami, K. K. Koziol, and A. H. Windle, ACS Nano **6**, 7723 (2012).
[58]S. W. Pattinson, R. D. Rivas, N. Stelmashenko, A. H. Windle, C. Ducati, E. A. Stach, and K. K. Koziol, Chem. Mater. **25**, 2921 (2013).
[59]K. K. Koziol, C. Ducati, and A. H. Windle, Chem. Mater. **22**, 4904 (2010).
[60]D. Young, J. Zhang, C. Geers, and M. Schütze, Mater. Corros. **62**, 7 (2011).
[61]A. Schneider, Corros. Sci. **44**, 2353 (2002).
[62]T. Thurakitseree, C. Kramberger, A. Kumamoto, S. Chiashi, E. Einarsson, and S. Maruyama, ACS Nano **7**, 2205 (2013).
[63]Z. Zhu, H. Jiang, T. Susi, A. G. Nasibulin, and E. I. Kauppinen, J. Am. Chem. Soc. **133**, 1224 (2010).
[64]R. M. Sundaram, K. K. Koziol, and A. H. Windle, Adv. Mater. **23**, 5064 (2011).
[65]L. Zhang, P.-X. Hou, S. Li, C. Shi, H.-T. Cong, C. Liu, and H.-M. Cheng, J. Phys. Chem. Lett. **5**, 1427 (2014).
[66]V. Reguero, B. Aleman, B. Mas, and J. J. Vilatela, Chem. Mater. **26**, 3550 (2014).